SCIENTIFIC REPORTS

OPEN

SUBJECT AREAS:
BATTERIES
NANOPARTICLES
SYNTHESIS AND PROCESSING
NANOSCALE MATERIALS

Received
4 September 2012

Accepted
19 November 2012

Published
17 December 2012

Correspondence and requests for materials should be addressed to Q.W.C. (cqw@ustc.edu.cn)

$CoMn_2O_4$ Spinel Hierarchical Microspheres Assembled with Porous Nanosheets as Stable Anodes for Lithium-ion Batteries

Lin Hu, Hao Zhong, Xinrui Zheng, Yimin Huang, Ping Zhang & Qianwang Chen

Hefei National Laboratory for Physical Sciences at Microscale and Department of Materials Science & Engineering, University of Science and Technology of China, Hefei, 230026, P. R. China.

Herein, we report the feasibility to enhance the capacity and stability of $CoMn_2O_4$ anode materials by fabricating hierarchical mesoporous structure. The open space between neighboring nanosheets allows for easy diffusion of the electrolyte. The hierarchical microspheres assembled with nanosheets can ensure that every nanosheet participates in the electrochemical reaction, because every nanosheet is contacted with the electrolyte solution. The hierarchical structure and well interconnected pores on the surface of nanosheets will enhance the $CoMn_2O_4$/electrolyte contact area, shorten the Li^+ ion diffusion length in the nanosheets, and accommodate the strain induced by the volume change during the electrochemical reaction. The last, hierarchical architecture with spherical morphology possesses relatively low surface energy, which results in less extent of self-aggregation during charge/discharge process. As a result, $CoMn_2O_4$ hierarchical microspheres can achieve a good cycle ability and high rate capability.

Nowadays, lithium-ion batteries have been employed for large-scale applications in various fields, such as hybrid and plug-in hybrid electric vehicles, solar and wind electricity generation systems. To meet the requirements of these applications, further improvements in terms of energy power, densities and cycle time are required. However, conventional bulk electrode materials display their inherent limits in performance and unable to fully reach the increasing demands. Nanostructured materials have attracted great interest in recent years for lithium batteries due to their promising electrical properties[1–5]. However, the capacity also fades rapidly under high current because nanoparticles are often self-aggregated because of their high surface energy, which reduces the effective contact areas of active materials, conductive additives and electrolyte. The huge volume changes of nanoaprticles due to Li^+ insertion and extraction also result in low capacity with cycle increasing. These intrinsic disadvantages have hindered widespread practical realizations of nanomaterials. On the other hand, although nanoelectrodes for lithium ion batteries possess many advantages, including improved cycling life, high effective electrode/electrolyte contact areas, short path length and so on, the potential disadvantages associated with the development of nanostructure for lithium ion batteries should be also stressed. Among them, the greatest disadvantage is the possibility of significant sub reactions with the electrolyte due to high external surface area, leading to safety concerns (one of the most critical issues for lithium ion batteries) and poor calendar life[6]. These problems may be improved with secondary nanomaterials that the particles are typically of micrometer dimensions but internally consist of nanometre-sized regions or domains, which could not only reduce side reactions with the electrolyte, but also can have the advantage of ensuring excellent electrical properties. In this regards, to some extent, micrometer-sized hierarchical mesoporous structures composed by nanometre-sized subunits can be taken as secondary nanomaterials, is one of the most ideal structures as cathode/anode materials for high-performance lithium ion batteries. Therefore, this structure can exploit many advantages of nanostructure for lithium ion batteries due to the reducing of side reactions with the electrolyte, leading to high density and long calendar life with few safety risks.

Over the past decade, various materials have been employed as anodes in Li-ion batteries, such as carbon[7], Sn[8], Si[9], transition metal oxides and so on. Carbon can store one lithium ion for every six carbon atoms through a staging mechanism corresponding to a theoretical capacity of only 372 mA h g^{-1}, which can not meet the requirements in many application fields. Although non-carbonaceous materials Sn and Si anodes deliver higher

capacities than carbon, unfortunately, there is a problem that their cycle life is poor because of materials disintegration due to the significant volume expansion during the charge and discharge cycling of Li ions. Among transition metal oxides, Co_3O_4 has attracted considerable attention in Li-ion rechargeable batteries field[10,11]. However, Co_3O_4 are not ideal anode materials in practical application because of their high cost, toxicity, and high lithium redox potential (2.2–2.4 V vs. Li^+/Li)[12]. Since manganese is more environmentally benign, much cheaper (manganese is 20 times less expensive than cobalt), more abundant in nature compared to cobalt, and available through current production, we are much more interested in replacing Co_3O_4 partially by eco-friendly and cheaper manganese. Manganese-based spinel nanomaterials are important technological materials because they have a wide range of applications as storage, magnetic resonance imaging, sorbents, drug delivery, battery materials, catalysts and so on[13–16]. Anode materials for Li-ion batteries based on spinel AMn_2O_4 (A = Co, Ni, and Zn) series have been investigated previously. Especially, interesting capacities for Li-ion batteries application of micro-structured $ZnMn_2O_4$ have been shown, such as 607 mA h g^{-1} for $ZnMn_2O_4$ hollow microspheres at 400 mA g^{-1} [12], 750 mA h g^{-1} for $ZnMn_2O_4$ ball-in-ball hollow microspheres at 400 mA g^{-1} and 690 mA h g^{-1} for $ZnMn_2O_4$ powders[17,18]. For the first time, Fabrice M. Courtel *et al* reported the performance of the AMn_2O_4 (A = Co and Ni) powders as anode material for Li-ion batteries, which demonstrated that $CoMn_2O_4$ and $NiMn_2O_4$ exhibited the poor performance, compared to the $ZnMn_2O_4$ powders[18]. The $CoMn_2O_4$ powders only exhibited a capacity of 515 mAh g^{-1} with retention of about 64% at a current of 69 mA g^{-1} after 50 cycles. Recently, Lou et al. reported double-shelled $CoMn_2O_4$ hollow microcubes achieved a capacity of 624 mAh g^{-1} with retention of about 75.5% at a current of 200 mA g^{-1} after 50 cycles[19]. Among the manganese spinels, $Mn_xCo_{3-x}O_4$ ($0 \leq x \leq 3.0$) crystallizes in cubic form (space group *Fd3m*) between $0 < x < 1.4$, and a tetragonal *(I41/amd)* spinel structure between $1.4 < x < 3.0$[20,21]. More interesting, their physicochemical properties highly depend on the composition, structural parameters, distribution and oxidation state of cations, which greatly affected by the synthesis conditions[22,23]. The traditional synthesis of spinel compounds is generally followed by a solid-state route involving, grinding and firing of a mixture of oxides, nitrates or carbonates, which requires elevated temperatures or prolonged process times to overcome the diffusional barriers. Therefore, these methods are not consistent with the low cost idea. Moreover, sol-gel processing[24], organic co-precipitation[25], flux or solvothermal strategies[26] and thermal decomposition method have been developed to replace the conventional ceramic preparations, which can proceed at moderate temperatures and form metastable phases because of enhanced reaction kinetics. Recently, Lou et al. reported the fabrication of $CoMn_2O_4$ hollow microcubes by thermal decomposition of $Co_{0.33}Mn_{0.67}CO_3$[19]. Despite continuous efforts, types of $CoMn_2O_4$ nanostructures reported are rather limited at current research.

Results

Inspired by the superiority of hierarchical mesoporous structure, in this report, for the first time, we demonstrate the fabrication of $CoMn_2O_4$ hierarchical microspheres assembled with porous nanosheets by a facile solvothermal synthesis and thermal decomposition method (Figure 1). The first step consists of precipitating metal alkoxide powders from ethanediol solutions of salts. The second step involves thermal decomposition under air, leading to crystalline spinel. The morphology of the precursor can be well preserved during thermal transformation from the precursor to $CoMn_2O_4$ hierarchical microspheres. Ethylene glycol (EG) is an optimal solvent that possesses good coordinating ability, and serves as a ligand to form coordination complexes with Co(II) and Mn(II) cations upon heating. The glycolate precursor connects each other during heating and the sheet morphology is formed due to van der Waals interactions. As-formed nanosheets will further aggregate into hierarchical spheres at appropriate conditions, driven by the minimization of interfacial energy[27–29], The different properties of the used organic solvents, such as polarity, viscosity and coordinating ability may be significant in the shape control of the precursor. Owing to the release of gases in the process of thermal treatment, the porous nanostructure is effectively obtained finally.

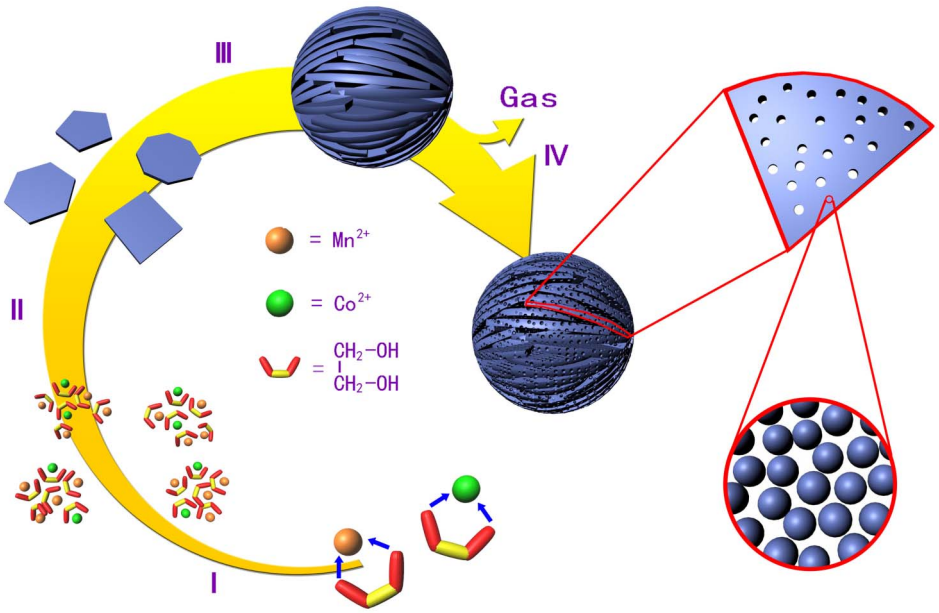

Figure 1 | Schematic illustration of the formation of $CoMn_2O_4$ hierarchical mesoporous microspheres. (I) formation of aggregations (Co-EG/Mn-EG); (II) formation of nanosheets; (III) formation of hierarchical microspheres of precursor; (IV) formation of $CoMn_2O_4$ hierarchical mesoporous microspheres by thermal decomposition, the porous nanostructure could be obtained due to the release of gases. Hierarchical structure means that the structure fabricated by smaller subunits. In our case, the hierarchical mesoporous microspheres are composed of porous nanosheets assembled by nanometre-sized crystalline.

The precursor phase formed in solvothermal reaction was first characterized by X-ray diffraction (XRD). Figure S1 shows the crystalline of the precursor, which is similar to the XRD patterns of Co-EG, Zn-Co-EG and Fe-EG[30–32]. It is hypothesized that a metal hydroxide could be formed and crystallized together with organic ligands in an alkaline environment under the solvothermal conditions. Indeed, the strong peak at around 10° is characteristic of products formed during polyol-mediated processes, which here could be ascribed to the formation of metal glycolates or alkoxide derivatives by alcoholysis and coordination of ethylene glycol with the metal ions. Basically, the precipitation of the alkoxides is highly dependent on the nature of the anionic composition of the medium. These anionic species can be hydroxide, acetate, or totally/partially deprotonated alcohols resulting from acid-base equilibrium reactions. In the presence of alkali and high pressure condition (solvothermal method), the main reactions are:

$$CH_3COO^- + H_2O \leftrightarrow CH_3COOH + OH^- \quad (1)$$

$$(CH_2OH)_2 + 2OH^- \leftrightarrow (CH_2)_2(O^-)_2 + 2H_2O \quad (2)$$

$$(CH_2)_2(O^-)_2 + Mn^{2+} \rightarrow (CH_2)_2(O)_2Mn\downarrow \quad (3)$$

$$(CH_2)_2(O^-)_2 + Co^{2+} \rightarrow (CH_2)_2(O)_2Co\downarrow \quad (4)$$

In addition, the precursor is characterized by thermogravimetric analysis (TG). Figure S2 shows a sharp mass loss from room temperature to 300°C in air. According to the TG curve, we chose a temperature of 600°C for thermal treatment of the precursor to ensure its complete decomposition. The XRD pattern of the final product is shown in Figure 2. Except the typical diffraction peaks of $CoMn_2O_4$ (JCPDS: 77-0471), three weak impurity peaks still can be found. These peaks marked by * can be indexed to Mn_2O_3. Compared with the intensity of $CoMn_2O_4$ peaks, Mn_2O_3 peaks are very weak, indicating the low content of Mn_2O_3. Moreover, it is well known that the electrochemical performance of Mn_2O_3 is poor, compared to that of the $CoMn_2O_4$. Therefore, we deduce that the impurity plays a negligible role on electrochemical performance discussed in the following. Based on Scherrer formula ($D = 0.89\lambda/B\cos\theta$) and XRD data (Figure S3), an average crystalline size of 21 nm is estimated from (211) peak (the strongest peak).

Figure S4 shows the general scanning electron microscopy (SEM) morphology of the as-prepared precursor obtained after solvothermal treatment. The low-magnification SEM image (Figure S4a) reveals that the product is composed of a great deal of microspheres with diameters of 4–6 μm. The high-magnification SEM image and the inset (Figure S4b) further indicate that these microspheres are assembled by nanosheets without serious aggregation. After thermal treatment at 600°C for 3 h in air, the as-prepared precursors can completely transform into $CoMn_2O_4$ (Figure 2). It should be noted that the hierarchical microstructures are quite thermally stable without structural collapse (Figure 3). The nanosheets possess a relatively high thickness of about 350 nm (Figure 3d), which can effectively ensure architecture stability. Therefore, even after thermal decomposition at 600°C for 3 h, the $CoMn_2O_4$ product still maintains the structure and morphology integrity. Interestingly, nanosheets intercross loose and obvious open space between neighboring nanosheets can be seen from the Figure 3d as shown by red arrows. The microstructure of the product was further investigated by TEM and HRTEM techniques. Figure 4a is the TEM image of a randomly selected microsphere, which displays regular spherical morphology. Many pores can be clearly seen from the edge of microsphere as shown by arrows in Figure 4a (white dots). The interlayer distance of randomly selected nanoparticle is calculated to be 0.302 nm and 0.285 nm, which agrees well with the (112) and (200) lattice plane, as shown in Figure 4b. The Mn/Co ratio determined by energy-dispersive X-ray spectroscopy (EDX) analysis is 2 (Figure 4c), which perfectly agrees with that in $CoMn_2O_4$. The porosity of the $CoMn_2O_4$ hierarchical microspheres is further characterized by N_2 sorption at 77 K (Figure S5). BET surface area data is calculated to be about 8 $m^2\ g^{-1}$ with a wide pore size distribution ranging from 2–120 nm. The release of gases during thermal treatment results in small pores in nanosheets, while the large pores can be attributed to the open space between neighboring nanosheets. Meanwhile, some of the small pores may connect with each other (distinct from "dead pores"), generating larger pores with a wide size distribution.

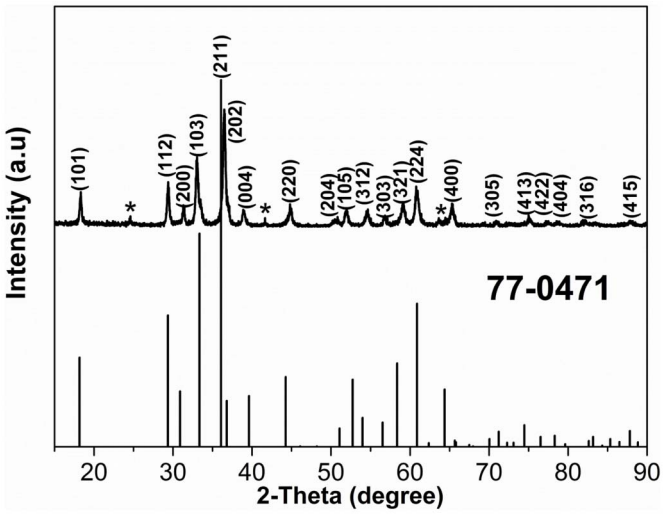

Figure 2 | Composition characteristic of the $CoMn_2O_4$ hierarchical microspheres. XRD pattern of the $CoMn_2O_4$ hierarchical microspheres.

Discussion

Considering that electrodes with special hierarchical porous nanostructures are advantageous to lithium-ion batteries, we investigate the lithium storage properties of as-prepared $CoMn_2O_4$ hierarchical microspheres using the standard $CoMn_2O_4$/Li half-cell configuration. Figure 5 demonstrates the first three consecutive cyclic voltammograms (CVs) of the electrode made by $CoMn_2O_4$ hierarchical microspheres. Three reduction peaks can be found in the cathodic polarization process of the first cycle. The broad peak centered at 1.06 V may be attributed to the reduction of Mn^{3+} to Mn^{2+}; the intense peak located at 0.36 V could be assigned to the further reduction of Mn^{2+} and Co^{2+} to metallic Mn and Co, respectively; while the minor peak at 0.76 V can be ascribed to the irreversible decomposition of the solvent in the electrolyte to form the solid-electrolyte interface (SEI). There are two oxidation peaks in the following anodic sweep; the one at 1.36 V is due to the oxidation of Mn to Mn^{2+}, while the other one at 2.00 V is caused by the oxidation of Co to Co^{2+}. The second cycle is characterized by two pairs of distinct redox peaks. The one at 0.53/1.47 V corresponds to the reduction/oxidation of MnO, while the other one at 1.05/2.04 V corresponds to the reduction/oxidation of CoO[19]. From the second cycle onwards, the CV curves are mostly overlapped, which indicates the good reversibility of the electrochemical reactions. Based on above analysis, the lithium insertion and extraction reactions for our porous $CoMn_2O_4$ electrode are believed to proceed as follows:

$$CoMn_2O_4 + 8Li^+ + 8e^- \leftrightarrow Mn + Co + 4Li_2O \quad (5)$$

Figure 5b shows discharge-charge curves of the electrodes made from the $CoMn_2O_4$ hierarchical microspheres at a current density of 100 mA g^{-1} at room temperature in a potential window between 0.01 and 3.0 V (vs. Li^+/Li). It can be seen that there is a large deviation in potential between charge and discharge curves. The gap between charge and discharge curves is important, which involves the energy efficiency. The large gap may be a feature of metal oxide anode due to the polarization related to ion transfer during charge-discharge cycles[33]. This phenomenon is often observed in many metal oxide anodes due to poor electrical conductivity[34], including

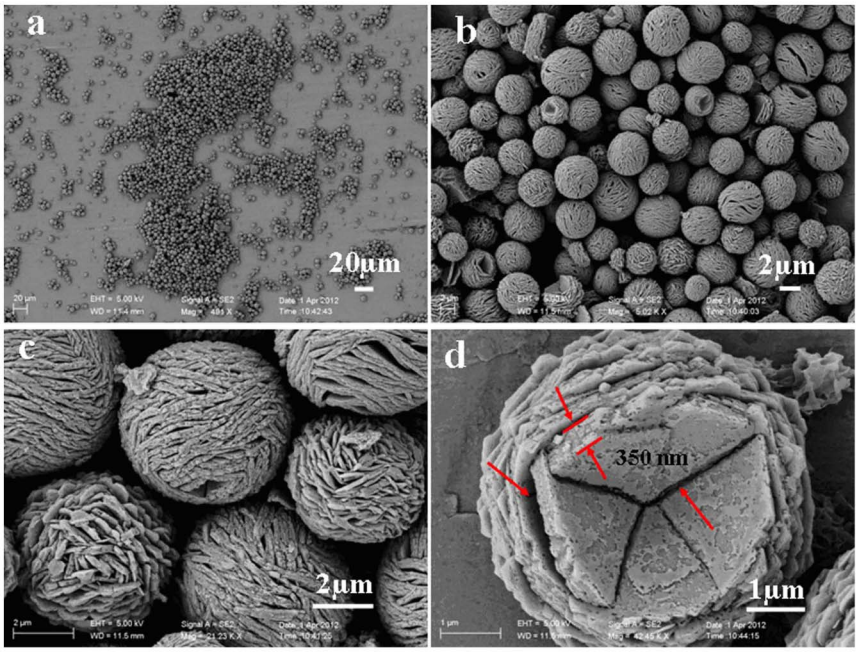

Figure 3 | Morphological and structural analysis of $CoMn_2O_4$ hierarchical microspheres. SEM images of the $CoMn_2O_4$ hierarchical microspheres at different magnifications.

$CoMn_2O_4$ reported previously[19]. It is reported that the incorporation of graphene sheets can partly reduce the voltage polarization[33]. The solution can be further studied in the future. The initial discharge and charge capacities are 1442 and 937 mAh g^{-1}, which is higher than the theoretical value (920 mAh g^{-1}) based on the conversion reaction (see equation 5). The excess capacities could be associated with the decomposition of the electrolyte at low voltages generating a solid electrolyte interphase (SEI) layer and the further lithium storage via interfacial charging at the metal/Li_2O interface. The large irreversible capacity loss of the first cycle can be attributed to the phenomenon that the formed SEI film can not completely decompose during the first charge.

Figure 5c shows the discharge/charge capacity versus cycle number for the electrodes made from the $CoMn_2O_4$ hierarchical microspheres at a current of 100 mA g^{-1}. It is interesting to observe that the discharge capacity decreases only slightly before 36 cycles. After that, more interestingly, an unusual phenomenon that the discharge capacity gradually increases to 900 mAh g^{-1} can be seen. This capacity is very close to the theoretical value of a fully reversible conversion reaction (920 mAh g^{-1}). Generally, after charge and discharge at a low current, the electrolyte penetrates into inner part of active materials. In our case, the current density of 100 mA g^{-1} is not very high. So, to some extent, the above situation may also happen, making inner part of $CoMn_2O_4$ also involved in the conversion reactions, and then results in the increase of capacity. On the other hand, the phenomenon that the discharge capacity gradually increases also attributes to progressive generation of electro-chemistry active polymeric gel-like films. Not all the surface layer is covered on the first discharge. The internal surface within the pores is more difficult to access. It would appear that the polymer layer builds-up slowly, over a number of cycles[35,36]. Of course, the specific reasons need to be studied further. After 65 cycles, this discharge capacity can be retained at 894 mAh g^{-1}, corresponding to 94.9% of the second discharge capacity (942 mAh g^{-1}), indicating excellent cycling stability. These above results are better than those in previous reports. It has been reported that $CoMn_2O_4$ hollow microcubes achieved a capacity of 624 mAh g^{-1} with retention of about 75.5% at a current of 200 mA g^{-1} after 50 cycles[19], while $CoMn_2O_4$ powders only exhibited a capacity of 515 mAh g^{-1} with retention of about 64% at a current of 69 mA g^{-1} after 50 cycles[18].

Because the rate capability is an important parameter for many applications of batteries such as electric vehicles and portable power tools, which require fast discharge and/or charge rate. We also investigate its rate performance with respect to Li^+ insertion/extraction. In order to evaluate the rate capability, the $CoMn_2O_4$ electrode is cycled at various current densities (0.1 C–10 C, 1 C = 900 mA g^{-1}) and the charge/diacharge curves are shown in Figure 5d. The cell shows good rate capability with average discharge capacity of 1129, 822, 694, 559,

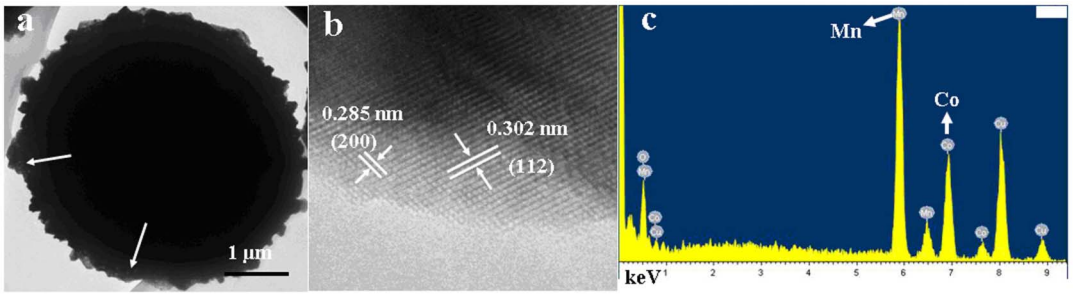

Figure 4 | Morphological and elemental analysis of $CoMn_2O_4$ hierarchical microspheres. (a, b) TEM and HRTEM images of $CoMn_2O_4$ hierarchical microspheres. (c) EDS spectrum of the $CoMn_2O_4$ hierarchical microspheres.

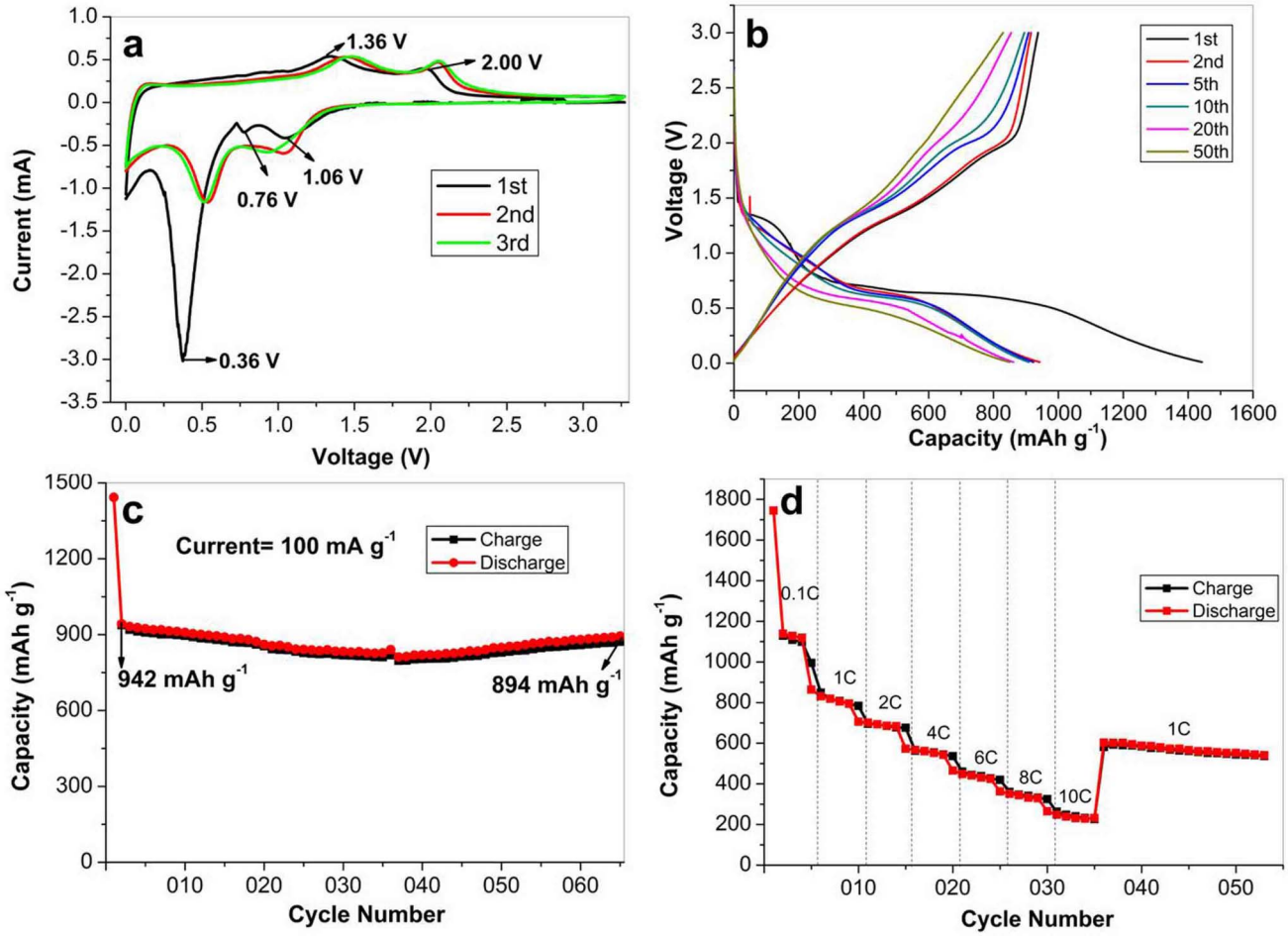

Figure 5 | Electrochemical properties of the $CoMn_2O_4$ hierarchical microspheres for lithium storage. (a) The first three consecutive CVs of the electrode made from $CoMn_2O_4$ hierarchical microspheres. (b) discharge-charge curves at a current of 100 mA g^{-1}. (c) Cycling performance of the $CoMn_2O_4$ hierarchical microspheres at a current of 100 mA g^{-1}. (d) Cycling performance of the $CoMn_2O_4$ hierarchical microspheres at various current rates from 0.1 C to 10 C (1 C = 900 mA g^{-1}). As for a half cell, the discharge process corresponds to the Li^+ insertion for $CoMn_2O_4$ reduction reaction, while the charge process corresponds to Li^+ extraction for $CoMn_2O_4$ oxidation reaction.

442, 344, 241 mA h g^{-1} at current densities of 0.1 C, 1 C, 2 C, 4 C, 6 C, 8 C and 10 C, respectively. While altering the current density back to 1 C, a discharge capacity of as high as 600 mA h g^{-1} could be recovered. As we can see, the capacity is comparable to that of commercially used graphite (372 mA h g^{-1}) even at the current of 6 C. Although $CoMn_2O_4$ hollow microcubes exhibit relative high capacity at a current of 200 mA g^{-1} (Retaining 624 mA h g^{-1} after 50 cycles)[19], the high rate capability is not present. However, the high rate capability of material is a significant factor for lithium-ion batteries, which can reduce lots of charge/discharge time in a practical application. To the best of our knowledge, this is the first report on the capacity of $CoMn_2O_4$ at such high currents. The good rate capability demonstrates the $CoMn_2O_4$ hierarchical microspheres have a great potential as a high-rate anode material in lithium ion batteries.

The power capability and rate performance of transition metal oxides electrode material mainly depend on the kinetics of the redox reactions processes, which involves lithium ion and electron diffusion to/from the electrolyte/particle interface[37]. Diffusions of lithium ions and electrons are complex because the nature of the electrolyte phase, the solid-liquid interface, the tortuosity of diffusion paths and the size of the nanoparticles need to be considered[5]. Nanostructured mesoporous materials can provide short path lengths with less for resistance both Li ion and electron transport within electrolyte. These compounds often exhibiting high diffusion coefficients show improved electrochemical properties, such as storage capacity, cycle stability and high current charge/discharge. Furthermore, it is well known that the electrochemical performance of battery strongly depends on the sizes and morphologies of electrode materials[38]. Based on points above, micron-sized hierarchical spherical materials with suitable porous structure can not only increase their energy densities, but also improve their rate capabilities. We believe the high capacity and rate capability of the $CoMn_2O_4$ hierarchical microspheres originate from the unique hierarchical mesoporous architecture. First, the open space between neighboring nanosheets allows for easy diffusion of the electrolyte (Figure 6a). This feature is particularly helpful for high power applications when the battery is charged or discharged at high current. Second, the hierarchical microspheres assembled with nanosheets can ensure that every nanosheet participates in the electrochemical reaction, because every nanosheet is contacted with the electrolyte solution (Figure 6b). Third, the hierarchical structure and well interconnected pores on the surface of nanosheets will enhance the $CoMn_2O_4$/electrolyte contact area, shorten the Li^+ ion diffusion length in the nanosheets, and accommodate the strain induced by the volume change during the electrochemical reaction. The last, hierarchical architecture with spherical morphology possesses low surface energy, which results in less extent of self-aggregation during charge/discharge process. As a result, $CoMn_2O_4$ hierarchical microspheres can achieve a good cycle ability and high rate capability. Based on our result, it can be concluded that the capacity of anode

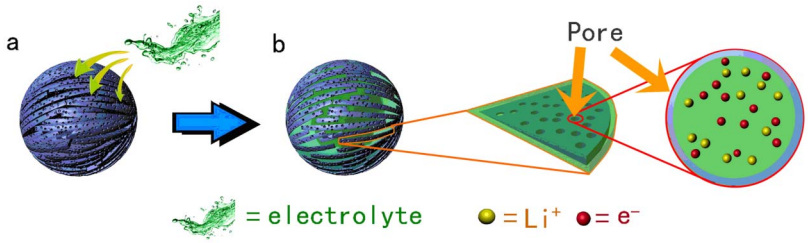

Figure 6 | Schematic illustration of the diffusion of electrolyte, electron and Li^+. (a) The electrolyte can diffuse into the inner part of $CoMn_2O_4$ hierarchical mesoporous microspheres easily from the open space between neighboring nanosheets. (b) Hierarchical structure can ensure that every nanosheet contact electrolyte, the pores between $CoMn_2O_4$ nanoparticles can ensure that Li^+ and electron diffuse with little resistance.

can be indeed improved by designing the hierarchical mesoporous nanostructure.

In order to further reveal the transport kinetics for the electrochemical properties of $CoMn_2O_4$ sample, alternating current impedance (AC) measurements are carried out after different cycles of discharge and recharge at 100 mA g^{-1} (Figure 7a). The measured cell is charged to 3 V, and then placed for a period of time to reach a stable state about 1.9 V for impedance measurement. The plots consist of a depressed semicircle in the high and middle frequency regions and a straight line in the low-frequency region. The semicircle at high frequency can be assigned to the SEI film and contact resistance (R_{SEI}), while that at mid-frequency is attributed to the charge-transfer impedance on electrode–electrolyte interface (R_{ct}). The linear region corresponds to the semi-infinite diffusion of the Li-ions in the $CoMn_2O_4$ electrodes (R_e)[39]. The impedance of fresh cell is smaller than that of first cycle, which further proves the formation of SEI film after first cycle. It is can be seen that the cell impedance slowly increasing with the cycle process, which is a normal phenomenon in many anode materials, such as graphite and MoO_2/graphene[40,41]. Small changes of R_{ct} and R_e have been shown from the plots, which imply that the diffusions of the Li-ions and electrons are also relatively convenient with cycle increasing. With the elongation of storage time, electrolyte partially begins to decompose and continuously to form the precipitation on the $CoMn_2O_4$ surface, resulting in the thicker SEI film and higher R_{SEI}. The slight increase of the R_{ct} and R_e during the storage time may be owing to the organic and/or polymeric parts of the SEI film dissolve in the electrolyte, which can decrease the conductivity of electrolyte. In some previous reports[39], the cell impedance decreases with the cycles increasing. This phenomenon is likely due to pulverization process in which the particles will become smaller. Although the pulverization process increases the total surface area of electrode materials, the smaller particles will aggregate to lose activity because of large surface energy, resulting in the decay of capacity and lifetime. In our case, the hierarchical mesoporous nanostructure is relatively stable, which reduce the milling effect with the elongation of storage time, and then the lifetime can be ensured. Figure 7b compares Bode plots of the cell after different cycles. It is indicated that the impedances at frequencies above 10^1 Hz almost remained constant with cycles, while those at frequencies below 10^1 Hz slowly increased with the cycles.

Based on conversion reaction, the spinel structure may be amorphous after the first discharge-charge cycle. As shown from Figure S6, the mixture ($CoMn_2O_4$/carbon/PVDF) did not fall off from copper film after 10 cycles at 200 mA g^{-1}. Figure S7 is the XRD patterns of the mixture before cycling and cycled for 10 cycles. The mixture was compressed onto a copper foil to form a thin film, and then the film was taken from the copper foil for XRD characterization before cycling. As shown from Figure S7a, the peaks of $CoMn_2O_4$ can be clearly observed, indicating the existence of $CoMn_2O_4$ crystal structure. The broad diffraction band around 21° was aroused from carbon and PVDF. It should be noted that the cell is charged back to 3 V and the mixture is also separated from the copper foil for XRD characterization. Several weak broadened peaks can be seen from Figure S7b, which demonstrates that the crystal structure of $CoMn_2O_4$ may be converting into the amorphous state during the cycles. This phenomenon is normal for metal oxide anode, which wields little influence over electrical properties. More importantly, as shown from Figure 8, after 10 cycles at 200 mA g^{-1}, it is interesting that the morphology of $CoMn_2O_4$ has involved negligible changes (as shown by red arrows and the inset), which displays original morphology and good dispersity, confirming the attractive morphological stability. It is worth mentioning that the average crystalline size of 21 nm is relatively small. With decreasing particle size, an increasing proportion of the total number of atoms lies near or on

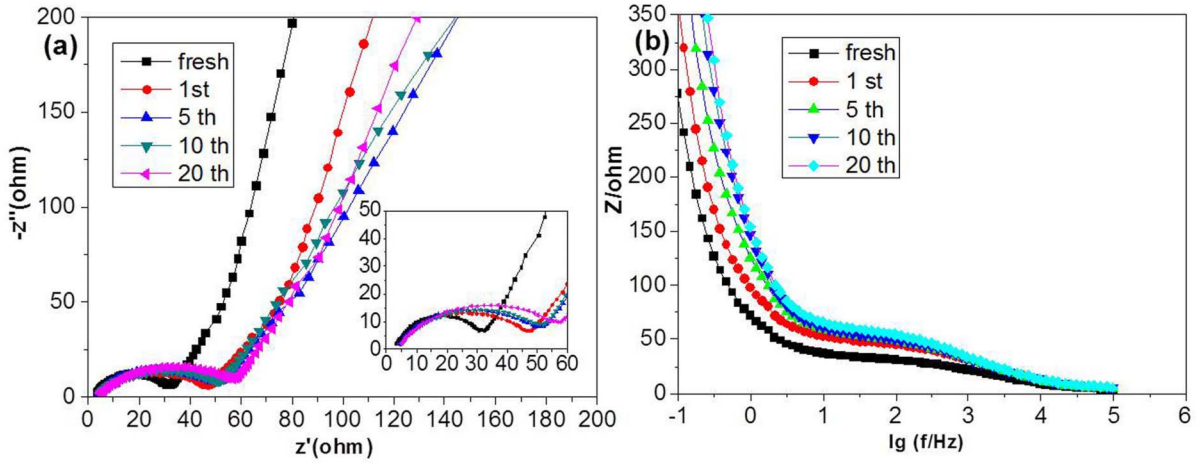

Figure 7 | Electrochemical impedance spectra and Bode plots of the $CoMn_2O_4$ hierarchical microsphere electrode. (a) The impedance spectra of $CoMn_2O_4$ electrode after different cycles of discharge and recharge at 100 mA g^{-1}. (b) Bode plots after different cycles.

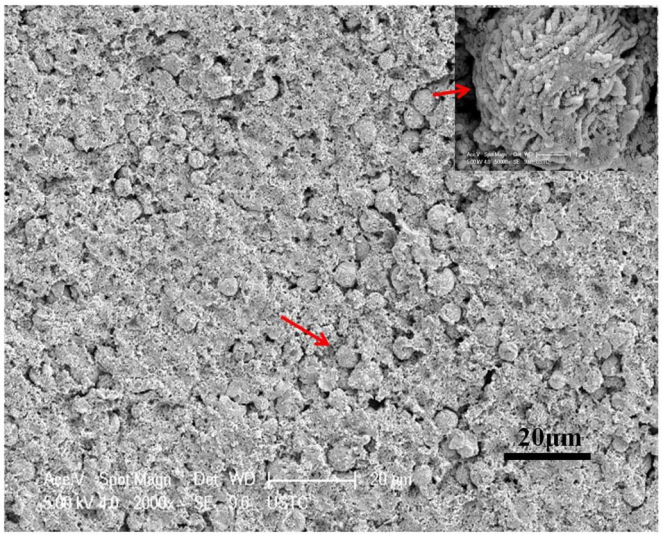

Figure 8 | Morphological analysis of the ($CoMn_2O_4$/carbon/PVDF) cycled for 10 cycles at a current of 200 mA g^{-1}. SEM images of the mixture.

the surface and enhances the surface Li storage. Especially, the capacity contributed by the surface Li storage is very stable upon cycling. Crystallinity is another important factor determining the electrochemical properties, and the improvement of crystallinity will lead to better cycling performance. In our previous paper[42], we have discussed the effect of crystallinity carefully. From the XRD pattern, we can see that the crystallinity of our product is similar to that of $CoMn_2O_4$ reported previously[19]. However, our product exhibits better electrochemical property, which indicating that the material's property is a result of mutilfactor determined. In our case, the hierarchical mesoporous nanostructure may play a more important role in determining electrochemical property.

In conclusion, we have developed a facile way to fabricate spinel $CoMn_2O_4$ hierarchical mesoporous microspheres. The resultant material have shown a high discharge capacity of 894 mAh g^{-1} at a current of 100 mA g^{-1} after 65 cycles, corresponding to 94.9% of the second discharge capacity (942 mAh g^{-1}), indicating excellent cycling stability. The good high rate capability demonstrates the $CoMn_2O_4$ hierarchical mesoporous microspheres have a great potential as a high-rate anode material in lithium ion batteries. We believe that their outstanding performance derived from the unique hierarchical architecture of the mesoporous nanosheets. Considering their ease of fabrication and good properties (cycling stability and high rate capability), these $CoMn_2O_4$ hierarchical mesoporous microspheres will hold promise in practical Li^+ ion batteries.

Methods

Synthesis of the $CoMn_2O_4$ hierarchical microspheres. All of the reagents used are of analytical purity and used without further purification. In a typical synthesis process, 1 mmol $Mn(CH_3COO)_2{\cdot}4H_2O$ (0.245 g), 0.5 mmol $Co(CH_3COO)_2{\cdot}4H_2O$ (0.124 g) and 1 g polyethylene glycol 1000 were dissolved in 35 ml ethylene glycol to form a clear solution. After being stirred vigorously for 10 min, the mixture was put into a 50 ml Teflon-lined stainless steel autoclave. The autoclave was treated at 200°C and maintained for 6 h before cooled in air. The resulting precipitates were filtered and washed several times with absolute ethanol and finally dried under oven at 60°C. These precipitates were calcined at 600°C for 3 h to obtain $CoMn_2O_4$ product.

Materials characterization. The obtained products were characterized on an X-Ray powder diffractometer with Cu Kα radiation (λ = 1.5406 Å) (Shimadzu Corporation, Japan). The morphology was examined with a JSM-6700F scanning electron microscope (SEM), the transmission electron microscope (TEM) was performed on a Hitachi model H-800 transmission electron microscope (TEM) at an accelerating voltage of 200 kV, and high-resolution transmission electron microscope (HRTEM) (JEOL-2011) was operated at an acceleration voltage of 200 kV. Thermogravimetric analysis (TGA) was carried out using a Shimadzu-50 thermoanalyser under air flow at 10°C min^{-1} in the temperature range 30–800°C. Specific surface areas were computed from the results of N_2 physisorption at 77 K (Micromeritics ASAP 2020) by using the Brunauer–Emmet–Teller (BET) and Barrett–Joyner–Halenda (BJH).

Electrochemical measurements. The electrochemical behavior of the $CoMn_2O_4$ hierarchical microspheres was examined using CR2032 coin type cells vs. Li with 1 M $LiPF_6$ in ethylene carbonate and diethyl carbonate (EC : DEC = 1 : 1, v/v) as the electrolyte. The working electrode was fabricated by compressing a mixture of the active materials, conductive material (acetylene black, ATB), and binder (polyvinylidene fluoride (PVDF)) in a weight ratio of $CoMn_2O_4$/carbon/PVDF= 50 : 30 : 20 onto a copper foil current collector. The cells were assembled in an argon-filled glove box (MBraun Labmaster 130). The electrode capacity was measured by a galvanostatic discharge-charge method at a current density of 100 mA g^{-1}. After different cycles, the impedance spectra of the same cell were measured on an electrochemical workstation (CHI 604 B) in the frequency range of 0.001–100 kHz.

1. Poizot, P., Laruelle, S., Grugeon, S., Dupont, L. & Tarascon, J. M. Nano-sized transition-metal oxides as negative-electrode materials for lithium-ion batteries. *Nature* **407**, 496–499 (2000).
2. Bruce, P. G., Scrosati, B. & Tarascon, J. M. Nanomaterials for rechargeable lithium batteries. *Angew. Chem. Int. Ed.* **47**, 2930–2946 (2008).
3. Wang, Z. Y., Zhou, L. & (David) Lou, X. W. Metal oxide hollow nanostructures for lithium-ion batteries. *Adv. Mater.* **24**, 1903–1911 (2012).
4. Zhou, L., Zhao, D. Y. & (David) Lou, X. W. $LiNi_{0.5}Mn_{1.5}O_4$ hollow structures as high-performance cathodes for lithium-ion batteries. *Angew. Chem. Int. Ed.* **51**, 243–245 (2012).
5. Jiang, C. H., Hosono, E. & Zhou, H. S. Nanomaterials for lithium ion batteries. *Nano. Today.* **1**, 28–33 (2006).
6. Aricò, A. S., Bruce, P., Scrosati, B., Tarascon, J. M. & Schalkwijk, W. V. Nanostructured materials for advanced energy conversion and storage devices. *Nat. Mater.* **4**, 366–377 (2005).
7. Masarapu, C., Subramanian, V., Zhu, H. W. & Wei, B. Q. Long-cycle electrochemical behavior of multiwall carbon nanotubes synthesized on stainless steel in lithium ion batteries. *Adv. Funct. Mater.* **19**, 1008–1014 (2009).
8. Nara, H., Fukuhara, Y., Takai, A., Komatsu, M., Mukaibo, H., Yamauchi, Y., Momma, T., Kuroda, K. & Osaka, T. Cycle and rate properties of mesoporous tin anode for lithium ion secondary batteries. *Chem. Lett.* **37**, 142–143 (2008).
9. McDowell, M. T., Lee, S. W., Ryu, I., Wu, H., Nix, W. D., Choi, J. W. & Cui, Y. Novel size and surface oxide effects in silicon nanowires as lithium battery anodes. *Nano. Lett.* **11**, 4018–4025 (2011).
10. Fan, Y. Q., Shao, H. B., Wang, J. M., Liu, L., Zhang, J. Q. & Cao, C. N. Synthesis of foam-like freestanding Co_3O_4 nanosheets with enhanced electrochemical activities. *Chem. Commun.* **47**, 3469–3471 (2011).
11. Yang, S. B., Feng, X. L., Ivanovici, S. & Müllen, K. Fabrication of graphene-encapsulated oxide nanoparticles: towards high-performance anode materials for lithium storage. *Angew. Chem. Int. Ed.* **49**, 8408–8411 (2010).
12. Zhou, L., Wu, H. B., Zhu, T. & (David) Lou, X. W. Facile preparation of $ZnMn_2O_4$ hollow microspheres as high-capacity anodes for lithium-ion batteries. *J. Mater. Chem.* **22**, 827–829 (2012).
13. Cheng, F. Y., Shen, J., Peng, B., Pan, Y. D., Tao, Z. L. & Chen, J. Rapid room-temperature synthesis of nanocrystalline spinels as oxygen reduction and evolution electrocatalysts. *Nat. Chem.* **3**, 79–84 (2011).
14. Hemberger, J., Lunkenheimer, P., Fichtl, R., Krug von Nidda, H.-A., Tsurkan, V. & Loidl, A. Relaxor ferroelectricity and colossal magnetocapacitive coupling in ferromagnetic $CdCr_2S_4$ *Nature* **434**, 364–367 (2005).
15. Fan, H. J., Knez, M., Scholz, R., Nielsch, K., Pippel, E., Hesse, D., Zacharias, M. & Gösele, U. Monocrystalline spinel nanotube fabrication based on the Kirkendall effect. *Nat Mater.* **5**, 627–631 (2006).
16. Matsuda, M., Ueda, H., Kikkawa, A., Tanaka, Y., Katsumata, K., Narumi, Y., Inami, T., Ueda, Y. & Lee, S. H. Spin-lattice instability to a fractional magnetization state in the spinel $HgCr_2O_4$. *Nat. Phys.* **3**, 397–400 (2008).
17. Zhang, G. Q., Yu, L., Wu, H. B., Hoster, H. E. & (David) Lou, X. W. Formation of $ZnMn_2O_4$ ball-in-ball hollow microspheres as a high-performance anode for lithium-ion batteries. *Advanced Materials* **24**, 4609–4613 (2012).
18. Courtel, F. M., Duncan, H., Abu-Lebdeh,Y. & Davidson, I. J. High capacity anode materials for Li-ion batteries based on spinel metal oxides AMn_2O_4 (A = Co, Ni, and Zn). *J. Mater. Chem.* **21**, 10206–10218 (2011).
19. Zhou, L., Zhao, D. Y. & Lou, X. W. Double-shelled $CoMn_2O_4$ hollow microcubes as high-capacity anodes for lithium-ion batteries. *Adv. Matetr.* **6**, 745–748 (2012).
20. Vila, E., Rojas, R. M., de Vidales, J. L. M. & Garcia-Martinez, O. Structural and thermal properties of the tetragonal cobalt manganese spinels $Mn_xCo_{3-x}O_4$ ($1.4 < x < 2.0$). *Chem. Mater.* **8**, 1078–1083 (1996).
21. Zhang, H. T. & Chen, X. H. Size-dependent x-ray photoelectron spectroscopy and complex magnetic properties of $CoMn_2O_4$ spinel nanocrystals. *Nanotechnology* **17**, 1384–1390 (2006).
22. Shoemaker, D. P., Li, J. & Seshadri, R. Unraveling atomic positions in an oxide spinel with two jahn−teller ions: local structure investigation of $CuMn_2O_4$. *J. Am. Chem. Soc.* **131**, 11450–11457 (2009).
23. Fierro, G., Ferraris, G., Dragone, R., Jacono, M. L. & Faticanti, M. H_2 reduction behavior and NO/N_2O abatement catalytic activityof manganese based spinels doped with copper, cobalt and iron ions. *Catal. Today.* **116**, 38–49 (2006).

24. Lavela, P., Tirado, J. L. & Vidal-Abarca, C. Sol–gel preparation of cobalt manganese mixed oxides for their use as electrode materials in lithium cells. *Electrochim. Acta* **52**, 7986–7995 (2007).
25. Rojas, R. M., Eladio, V., Oscar, G. & José L. M. V. Thermal behaviour and reactivity of manganese cobaltites $MnxCo_{3-x}O_4$ (0.0, x, 1.0) obtained at low temperature. *J. Mater. Chem.* **4**, 1635–1639 (1994).
26. Matsushita, Y., Ueda, H. & Ueda, Y. Flux crystal growth and thermal stabilities of LiV_2O_4. *Nat. Mater.* **4**, 845–850 (2005).
27. Cölfen, H. & Antonietti, M. Mesocrystals: inorganic superstructures made by highly parallel crystallization and controlled alignment. *Angew. Chem. Int. Ed.* **44**, 5576–5591 (2005).
28. Cölfen, H. & Mann, S. Higher-order organization by mesoscale self-assembly and transformation of hybrid nanostructures. *Angew. Chem. Int. Ed.* **42**, 2350–2365 (2003).
29. Cheng, Z. G. Wang, S. Z., Wang, Q. & Geng, B. Y. A facile solution chemical route to self-assembly of CuS ball-flowers and their application as an efficient photocatalyst. *CrystEngComm.* **12**, 144–149 (2010).
30. Chen, Y. C., Hu, L., Wang, M., Min, Y. L. & Zhang, Y. G. *Colloids Surf., A* **336**, 64–69 (2009).
31. Qiu, Y. C., Yang, S. H., Deng, H., Jin, L. M. & Li, W. S. A novel nanostructured spinel $ZnCo_2O_4$ electrode material: morphology conserved transformation from a hexagonal shaped nanodisk precursor and application in lithium ion batteries. *J. Mater. Chem.* **20**, 4439–4444 (2010).
32. Larcher, D., Sudant, G., Patrice, R. & Tarascon, J.-M. Some insights on the use of polyols-based metal alkoxides powders as precursors for tailored metal-oxides particles. *Chem. Mater.* **15**, 3543–3551 (2003).
33. Mai,Y. J., Shi, S. J., Zhang, D., Lu, Y., Gu, C. D. & Tu, J. P. NiO–graphene hybrid as an anode material for lithium ion batteries. *J. Power Sources.* **204**, 155–161 (2012).
34. Mai, Y. J., Xia, X. H., Chen, R., Gu, C. D., Wang, X. L. & Tu, J. P. Self-supported nickel-coated NiO arrays for lithium-ion batteries with enhanced capacity and rate capability. *Electrochim. Acta.* **67**, 73–78 (2012).
35. Park, J. C., Kim, J., Kwon, H. & Song, H. Gram-scale synthesis of Cu_2O nanocubes and subsequent oxidation to CuO hollow nanostructures or lithium-ion battery anode materials. *Adv. Mater.* **21**, 803–807 (2009).
36. Shaju, K. M., Jiao, F., Débart, A. & Bruce, P. G. Mesoporous and nanowire Co_3O_4 as negative electrodes for rechargeable lithium batteries. *Phys. Chem. Chem. Phys.* **9**, 1837–1842 (2007).
37. Liu, J., Conry, T. E., Song, X. Y., Doeff, M. M. & Richardson, T. J. Nanoporous spherical $LiFePO_4$ for high performance cathodes. *Energy Environ. Sci.* **4**, 885–888 (2011).
38. Deng, Y. F., Li, Z. E., Shi, Z. C., Xu, H., Peng, F. & Chen, G. H. Porous Mn_2O_3 microsphere as a superior anode material for lithium ion batteries. *RSC Advances.* **2**, 4645–4647 (2012).
39. Song, R. R., Song, H. H., Zhou, J. S., Chen, X. H., Wu, B. & Yang, H. Y. Hierarchical porous carbon nanosheets and their favorable high-rate performance in lithium ion batteries. *J. Mater. Chem.* **22**, 12369–12374 (2012).
40. Yang, S. B., Song, H. H., Chen, X. H., Okotrub, A. V. & Bulusheva, L. G. Electrochemical performance of arc-produced carbon nanotubes as anode material for lithium-ion batteries. *Electrochim. Acta.* **52**, 5286–5293 (2007).
41. Sun, Y. M., Hu, X. L., Luo, W. & Huang, Y. H. Self-assembled hierarchical MoO_2/graphene nanoarchitectures and their application as a high performance anode material for lithium-ion batteries. *ACS Nano.* **5**, 7100–7107 (2011).
42. Yan, N., Hu, L., Li, Y., Wang, Y., Zhong, H., Hu, X. Y., Kong, X. K. & Chen, Q. W. Co_3O_4 nanocages for high-performance anode material in lithium-ion batteries. *J. Phys. Chem. C.* **116**, 7227–7235 (2012).

Acknowledgements

This work was supported by the National Natural Science Foundation (NSFC, 21071137) and U1232211.

Author contributions

L.Hu and Q.W. Chen designed and carried out research, analysed data and wrote the paper. Other authors also contributed extensively to the work presented in this paper.

Additional information

Supplementary Information accompanies this paper at http://www.nature.com/scientificreports

Competing financial interests: The authors declare no competing financial interests.

How to cite this article: Hu, L. *et al.* $CoMn_2O_4$ Spinel Hierarchical Microspheres Assembled with Porous Nanosheets as Stable Anodes for Lithium-ion Batteries. *Sci. Rep.* **2**, 986; DOI:10.1038/srep00986 (2012).